Desalination and Water Treatment
www.deswater.com

doi: 10.5004/dwt.2020.25165

180 (2020) 95–103
March

Improvement of reverse osmosis process stability in internally staged design under seasonal variation of feed water

Seung Ji Lim[a], Kwanho Jeong[b], Yong-joo Cho[c], Jungsu Park[c], Taekuk Lee[c], Seo Jin Ki[d,*], Joon Ha Kim[a]

[a]*School of Earth Sciences and Environmental Engineering, Gwangju Institute of Science and Technology (GIST), Gwangju 500–712, Republic of Korea*
[b]*Singapore Membrane Technology Centre, Nanyang Environment and Water Research Institute, Nanyang Technological University, Singapore 637141, Singapore*
[c]*Hanwha Engineering and Construction (E&C), 76 Gajeong-Ro, Yuseong-Gu, Daejeon, 34128, Republic of Korea*
[d]*Department of Environmental Engineering, Gyeongnam National University of Science and Technology, 33 Dongjin-ro, Jinju-si, Gyeongsangnam-do 52725, Korea, Tel. +82-55-751-3341; Fax: +82-55-751-3484; email: seojinki@gntech.ac.kr*

Received 1 July 2019; Accepted 18 November 2019

ABSTRACT

In this study, we conducted a numerical simulation to evaluate stability in the seawater reverse osmosis (SWRO) process against seasonal variations of feed water. The impact of element configuration on SWRO operation was analyzed using a process model consisting of the solution–diffusion model. Seawater quality and temperature data collected from the intake of the Fujairah desalination plant (United Arab Emirates) were used to identify optimum internally staged design (ISD) configurations. Monitoring data were also used to simulate changes in SWRO performance. The process performance of the ISD configurations as compared to conventional design configurations in terms of specific energy consumption, permeate total dissolved solids concentration and recovery ratio. The results showed that SWRO processes with four ISD configurations met the performance requirements over 12 months despite the fluctuations in seawater quality and temperature. The prediction results of the ISD configurations showed stable operation during the 12 month simulation period. These configurations had a significant advantage with respect to membrane maintenance. This study's findings could be used to optimize the element configuration of the SWRO process by predicting the process performance while accounting for seasonal variations of seawater quality and temperature.

Keywords: Seawater reverse osmosis (SWRO); Internally staged design (ISD); Seasonal variation of seawater; Process performance; Cleaning frequency

1. Introduction

Seawater reverse osmosis (SWRO) is a technology that has recently drawn attention due to the advantages of using seawater as the main source for feed water [1]. Since its commercialization, a great deal of research has been conducted to improve its efficiency [2]. Three methods are often employed to improve the process performance and increase the energy efficiency of SWRO. First, improvements in the performance of the semi-permeable membrane used to purify the seawater enhance the overall SWRO performance. Water–solute selectivity increases the energy efficiency of the process by eliminating the additional processes needed to separate water and solute [3–5]. The membrane development and its modular scale-up for commercialization, however, have encountered several difficulties—in particular, the tradeoff relation of water and salt permeabilities is a critical hindrance to improve a membrane with both high water flux and high solute rejection [5]. Second, the design of

* Corresponding author.

This article was originally published with errors on page 96 and the list of references. This version has been updated.
Please see Corrigendum in vol. 270 (2022) 322 [doi: 10.5004/dwt.2022.29013].

the SWRO process is an important performance factor [6,7]. A one-stage SWRO system is enough to meet the designed process performance standards if the appropriate pretreatment process is used [8] or the overall water recovery is set to below 50% [9]. Finally, the optimization of operation and maintenance (O&M) in the SWRO process can play a supportive role in reducing the additional energy consumption caused by membrane fouling over a long period of filtration. As the membrane cleaning and replacement schedule affects process performance, it is important to decide when and how to clean the membrane properly [10,11]. In the design and O&M steps, SWRO optimization should take into account the seasonal variations of water quality and temperature in the target intake area [12–14].

Earlier studies showed that internally staged design (ISD) can be applied at both the design and operation stages of SWRO to improve the process's water recovery, energy consumption, and degradation of such performances over the operation time. ISD combines more than two types of membrane elements to configure a pressure vessel rather than a single membrane element. Its advantage over a single element configuration is that a smaller plant size is required [15]. This can reduce capital costs by 5%–8% [16]. In addition, operation costs, including expenditures for electricity, chemical agents for membrane cleaning, and membrane replacement, can be reduced by 0.7%–6.5% [15]. However, the use of a single type of SWRO membrane for an element configuration in a pressure vessel does not guarantee the optimal performance of the SWRO process. Therefore, different types of membrane elements must be combined for efficient ISD depending on the seawater quality and the target SWRO performance. For example, in the case of seawater with high fouling potential, a high rejection membrane should be used as the lead element [17]. If low energy consumption is required in the SWRO process, a high flux membrane should be included in the configuration [18]. Previous studies have focused on either numerical demonstrations of the benefits of ISD or on developing algorithms to search for optimum ISDs [15–18]. Their simulation conditions have generally been constant temperatures and total dissolved solids (TDS) concentrations over time. For a more practical simulation, however, it is important to use actual monitoring data, rather than inputting constant temperature or TDS concentrations into the developed algorithm.

In this study, we employed ISD to run the SWRO system efficiently under various seasonal variations of seawater quality and temperature. To this end, monitoring data of seawater quality and temperature were used as the input data for the ISD optimization algorithm to obtain optimal configurations. Then, the performance of the SWRO process with ISD configurations was compared to that of conventional design (CD) configurations. The algorithm used in this study was a modified version of a previously developed ISD optimization algorithm [17]. This algorithm included one of the famous optimization algorithms, the pattern search algorithm. The difference between this modified algorithm and the previous algorithm was that they were with and without temperature correction factors (TCF), respectively. In the modified algorithm, TCFs were applied to water permeability and salt permeability coefficients. Comparisons of the process performance were accessed in terms of specific energy consumption (SEC), permeate water quality, and recovery ratio. Finally, the effect of ISD configurations on the cleaning frequency was analyzed. In summary, the specific objectives of this study were (1) to propose an optimization algorithm for ISD configurations that could meet the performance requirements with monthly fluctuations in seawater quality and water temperature, (2) to compare process performance of SWRO models depending on the element configurations over the 12-month simulation period, and (3) to analyze the effect of the element configurations on the cleaning schedule.

2. Materials and methods

2.1. Feedwater variation in real plant

Fig. 1 illustrates the seasonal variations of seawater temperature and TDS concentration in the intake of the Fujairah desalination plant in the United Arab Emirates during 12 months of operation, from February 2006 to January 2007. Monitoring data consisted of 273 paired datasets of seawater temperature and TDS concentration in a daily format. Null data in the datasets were eliminated to avoid divergence of the SWRO model during simulation. The temperature and TDS concentration increased from February to a peak in August and then decreased to the end of the period. The TDS concentration had a maximum value of 36,585 mg/L and a minimum value of 38,219 mg/L. The temperature ranged between 23.1°C and 35.7°C. Monitoring data were utilized in two different ways. First, in the optimization step, the monthly average values of TDS concentration and temperature were employed to identify the optimum ISD configuration. In doing so, the optimization algorithm could reduce iteration steps and derive optimum element configurations for monthly fluctuations at a reasonable time. Second, daily values of temperature and TDS concentration were used to simulate the SWRO performance depending on the membrane configuration. The process performance was evaluated daily, as the simulation of the process model was undertaken daily. The number of datasets was increased from 273 to 365 using simple interpolation. It is noted that the monitoring data of the Fujairah desalination plant was previously employed to conduct simulation studies for the reverse osmosis process [19–22]. The part of

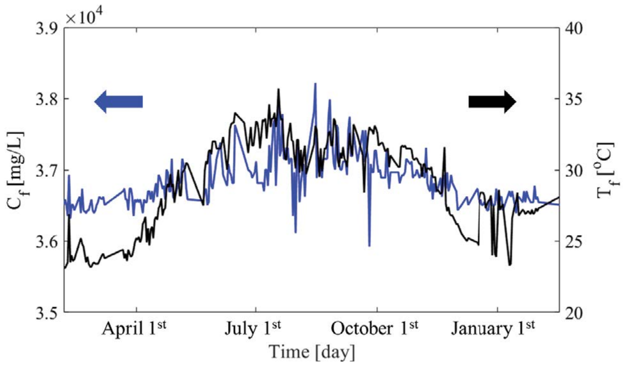

Fig. 1. Graphical illustration of seawater temperature and total dissolved solids (TDS) concentration in the intake of the Fujairah desalination plant during the 12-month observation period.

dataset, seawater temperature and TDS concentration in the intake of the Fujairah desalination plant, was employed in this study to consider seasonal variations of seawater quality in the simulation of reverse osmosis process.

2.2. SWRO process model considering temperature changes

We adopted the solution–diffusion model to numerically describe the transport of seawater in the membrane. This model uses two types of flux to represent the diffusive transport of water and salt taking place individually through the membrane. The water flux v_w and salt flux v_s are calculated as follows [23]:

$$v_w = A\left(\Delta p - \Delta\pi_m\right) \tag{1}$$

$$v_s = B\left(c_m - c_p\right) \tag{2}$$

where A is water permeability and B is salt permeability, Δp and $\Delta\pi$ denote transmembrane pressure and osmotic pressure difference, respectively, c_m refers to the TDS concentration at the membrane wall, and c_p is the permeate TDS concentration, which can be defined as v_s/v_w. Eqs. (1) and (2) can be modified to take temperature variation into account during the simulation. The modified equations are as follows [19]:

$$v_w = \frac{A}{\mathrm{TCF}_A}\left(\Delta p - \Delta\pi_m\right) = \frac{\Delta p - \Delta\pi_m}{\mu \cdot R_t \cdot \mathrm{TCF}_A} \tag{3}$$

$$v_s = B \cdot \mathrm{TCF}_B \cdot \left(c_m - c_p\right) \tag{4}$$

where TCF indicates a temperature correction factor. The TCF is multiplied by A and B. Thus, the model reflects the change in membrane properties with temperature variations. The subscripts in TCF represent the TCF for A and B. TCF equations have an exponential form [21]:

$$\mathrm{TCF}_A = \exp\left(a_T\left(\frac{1}{T} - \frac{1}{T_{\mathrm{ref}}}\right)\right) \tag{5}$$

$$\mathrm{TCF}_B = \exp\left(b_T\left(\frac{1}{T} - \frac{1}{T_{\mathrm{ref}}}\right)\right) \tag{6}$$

where a_T and b_T are the temperature coefficients for TCF_A and TCF_B, respectively. T_{ref} in this study was set to 298.15 K when A and B were calculated using the projection program of the membrane manufacturer at 298.15 K. Seawater viscosity μ with varying temperature can be calculated with an empirical equation [24]:

$$\mu = 2.414 \times 10^{-5} \times 10^{\frac{247.8}{T-140}} \tag{7}$$

where T is the seawater temperature in absolute temperature. A theoretical equation is used to calculate changes in osmotic pressure to temperature changes [25]:

$$\pi_m = \frac{N_{\mathrm{ion}} R_g T \Delta c_m}{M_s} \tag{8}$$

where N_{ion} denotes the number of ions, R_g is the gas constant, and M_s is the molecular weight of the solute.

In a process model, the crossflow velocity along the membrane channel is expressed as follows [19,26]:

$$u = u_0 - \frac{1}{H^*}\int_0^x v_w(\xi)\,d\xi \tag{9}$$

where u_0 is the crossflow velocity at the entrance of the membrane channel, and ξ is a dummy variable for the integration of distance x. H^* (=$H_0 - \delta_c$) denotes the effective height of the membrane channel and reflects the change in channel height from an initial channel height H_0 due to an increase in cake-layer thickness δ_c. Similarly, the transmembrane pressure is calculated using the following equation [19,26]:

$$\Delta p = \Delta p_0 - \frac{12 k_{\mathrm{friction}} \mu}{H^{*2}}\int_0^x u(\xi)\,d\xi \tag{10}$$

where Δp_0 is the transmembrane pressure at the entrance of the membrane channel, and k_{friction} is the friction coefficient for the channel wall and spacer in the membrane module. The TDS concentration in the membrane can be calculated using mass balance along the membrane channel:

$$c_x = \frac{1}{u_x}\left[u_0 c_0 - \int_0^x \frac{v_s}{H^*}\,d\xi\right] \tag{11}$$

where c_0 is the TDS concentration in the feed water.

2.3. Colloidal fouling and cake-enhanced osmotic pressure

Membrane resistance in the modified solution–diffusion model is calculated using the cake-layer deposition. The reciprocal of A is considered as membrane resistance. Colloidal fouling is assumed to be the main factor that increases membrane resistance. Therefore, the total membrane resistance is calculated by adding the intrinsic membrane resistance to the membrane resistance due to colloidal fouling:

$$R_t = R_m + R_c \tag{12}$$

$$R_c = \left[\frac{180(1-\varepsilon)}{\rho_p d_p^2 \varepsilon^3}\right] m_d \tag{13}$$

where ε is cake-layer porosity, ρ_p and d_p indicate the particle density and diameter of the colloidal foulant, respectively, and m_d represents the mass of the colloid deposit layer per membrane unit area. m_d can be calculated by integrating a net convective flux of foulant over time [27,28]:

$$m_d = k_{\mathrm{fp}}\int_0^t c_f\left(v_w - v_{\mathrm{crit}}\right)d\tau \tag{14}$$

where τ is a dummy variable for the integration of time t, k_{fp} denotes the colloidal fouling potential coefficient, and v_{crit} is the critical flux. It is assumed that colloidal foulant does not deposit on the membrane surface if v_w is smaller than v_{crit}. The empirical correlation of $v_{\mathrm{crit}} \sim u^{0.4}$ was employed to simulate the SWRO model [27]. The foulant concentration in the brine c_f is calculated as follow:

$$c_f = \frac{1}{u_x}\left[u_0 c_{f0} - k_{\text{fp}} \int_0^x \frac{c_f\left(v_w - v_{\text{crit}}\right)}{H^*} d\xi\right] \tag{15}$$

where c_{f0} indicates the foulant concentration in the inlet of the membrane channel.

The deposition of colloidal foulant leads to enhanced osmotic pressure at the membrane surface. Cake-enhanced osmotic pressure (CEOP) is a phenomenon wherein osmotic pressure increases due to the accumulation of colloidal foulant. CEOP is taken into account by considering the cake-hindrance effect on the mass transfer coefficient. The solute concentration at the membrane surface is expressed as follow [29]:

$$c_m = c_b \exp\left(\frac{v_w}{k^*}\right) \tag{16}$$

where k^* is the mass transfer coefficient under cake-hindrance. k^* is calculated by considering the change of mass transfer coefficient due to cake layers:

$$k^* = \left[\frac{m_d}{\rho_p(1-\varepsilon)}\left(\frac{\varepsilon}{\tau_c}\cdot\frac{1}{D_b} - \frac{1}{D_b}\right) + \frac{1}{k}\right]^{-1} \tag{17}$$

where D_b denotes the bulk diffusion coefficients of the solute. τ_c (=1−ln(ε^2)) is the cake-layer tortuosity. k is a mass transfer coefficient, which is determined using the following equation [30]:

$$k = \frac{\text{Sh}\cdot D_b}{d_h} \tag{18}$$

where d_h is the hydraulic diameter of the membrane channel. Sh indicates the Sherwood number with the empirical equations as follow:

$$\text{Sh} = 0.065\,\text{Re}^{0.875}\,\text{Sc}^{0.25} \tag{19}$$

where Re is the Reynolds number, and Sc is the Schmidt number.

2.4. Performance of the process model

The performance of the SWRO model was analyzed in terms of permeate TDS concentration, recovery ratio, and SEC. The permeate flow rate is calculated by integrating v_w with respect to the distance x from the entrance to the end of the membrane channel. The permeate TDS concentration can be calculated by dividing the integration of salt flux along the total length of channel TL by the permeate flowrate Q_p. The recovery ratio Rec is the ratio of the feedwater flow rate to the permeate flow rate [17]:

$$Q_p = \int_0^{\text{TL}} v_w w\,dx \tag{20}$$

$$c_p = \frac{\int_0^{\text{TL}} v_w c_p w\,dx}{Q_p} \tag{21}$$

$$\text{Rec} = \frac{Q_p}{Q_f} \tag{22}$$

where w is the membrane channel width. SEC is calculated by dividing the work done by the high-pressure pump W_{HP} and the booster pump $W_{\text{BP}}^{\text{ERD}}$ by the amount of produced water in the SWRO system [31]:

$$\text{SEC} = \frac{W_{\text{HP}} + W_{\text{BP}}^{\text{ERD}}}{Q_p} \tag{23}$$

$$W_{\text{HP}} = \left(p_f - p_{\text{in}}\right)\frac{\text{Rec}\times Q_f}{\eta_{\text{HP}}} \tag{24}$$

$$W_{\text{BP}}^{\text{ERD}} = \left(p_f - p_{\text{in}} - \eta_{\text{ERD}}\left(p_c - p_{\text{out}}\right)\right)\frac{Q_b}{\eta_{\text{BP}}} \tag{25}$$

where η_{HP} is the high-pressure pump's efficiency, η_{BP} indicates the booster pump's efficiency, and η_{ERD} is the efficiency of the energy recovery device (ERD). p_{in} and p_{out} denote feed pressure before the high-pressure pump and brine pressure after passing the ERD, respectively. Table 1 shows the values for each parameter used in the simulation. It is noted that c_p and SEC were used to determine the cleaning schedule in the SWRO model simulation. When the SEC or c_p values of the SWRO model reached 2.5 kWh/m^3 and 500 mg/L, respectively, membrane cleaning was performed. In the simulation, it was assumed that the recovery of membrane performance after cleaning was 100%. Therefore, the total membrane resistance was initialized to R_m after the cleaning simulation.

2.5. ISD optimization algorithm

Fig. 2 represents the procedure of the ISD optimization algorithm against fluctuations in temperature and TDS concentration. The first step is to load the membrane properties designated by a specific manufacturer from the membrane database, which contains the water permeability and salt permeability specifications of membranes from various manufacturers. After loading the membrane properties, the design conditions for the SWRO process are inputted into the algorithm, and the constraints for the optimization and performance requirements are set. Monthly mean seawater temperature and TDS concentration values are used to reflect seasonal temperature and quality variations. The number of monthly mean values determines the number of scenarios generated from the optimization algorithm. As noted, the previously developed ISD optimization algorithm utilizes the pattern search algorithm, which searches a single case that maximizes the permeate flow rate. This algorithm was modified to produce outputs for more than one element configuration during the iteration of the optimization algorithm. Thus, the optimization algorithm generates more than one element configuration for each scenario. Scenario studies were conducted for the monthly mean of seawater temperature and TDS concentration for 12 months, and 12 scenarios were generated. In the final step, a string search algorithm was used to find common ISD configurations among the 12

Table 1
Parameter values and target values used in internally staged design (ISD) optimization and simulation

Parameters	Values
SWRO model operating conditions	
Coefficient for TCF_A, a_T (*K*)	3,000
Coefficient for TCF_B, b_T (*K*)	–4,500
Feed flowrate, Q_f (m^3/d)	300
Feed pressure, P_f (bar)	65
Efficiency of high-pressure pump, η_{HP} (%)	85
Efficiency of booster pump, η_{BP} (%)	85
Efficiency of ERD, η_{ERD} (%)	95
Length of operation (d)	365
Membrane element properties	
Spacer thickness, H (m)	8.64×10^{-4}
Membrane channel width, w (m)	37
Membrane channel length, L (m)	1
Number of membrane elements in a pressure vessel	7
Hydrodynamic properties	
Diffusion coefficient of solute, D_b (m^2/s)	0.36
Friction coefficient due to the membrane spacer, K (–)	14
Cake-layer properties of colloidal fouling	
Porosity of the cake layer, ε (–)	0.36
Particle density of the foulant, ρ_p (kg/m^3)	1.4×10^3
Diameter of the foulant particle, d_p (nm)	20
Colloidal fouling potential, k_{fp} (–)	1.25
Foulant concentration (inlet), c_{f0} (mg/L)	10
Constraints for ISD optimization	
Maximum permeate concentration (mg/L)	500
Maximum specific energy consumption (kWh/m^3)	2.5

scenarios. The ISD configurations found were considered to meet every requirement for the monthly means of temperature and TDS concentration. The performance requirements were SEC with a maximum value of 2.5 kWh/m^3 and permeate TDS concentration with a maximum value of 500 mg/L. Four different membranes from the same manufacturer were used: two high flux and two high rejection.

3. Results and discussion

3.1. Element configurations from the optimization algorithm

Table 2 shows the number of ISD configurations generated by the optimization algorithm depending on the monthly fluctuations in temperature and TDS concentration. The changes in seawater properties affected the required number of adequate ISD configurations. The number of cases that met the design criteria decreased in correlation with the increase in temperature and TDS concentration, suggesting that it may be hard for ISD to meet the performance requirements at high temperatures and TDS concentrations. Only four ISD configurations from those of 12 scenarios were suitable to use for the SWRO model simulation because the performance of four ISD configurations satisfied the performance requirement (SEC ≤ 2.5 kWh/m^3 and $c_p \leq 500$ mg/L) over a period of 12 months. Table 3 presents the element configurations that were used. Although the number of membrane types used for element combinations was set to a maximum of three, the algorithm suggested configuring only two types of membrane (i.e., HR 1 and HF 2) for the optimal ISD. High rejection membranes were positioned at the lead of the pressure vessel (i.e., from the first two up to elements), and the remaining elements were filled with high flux membranes. Otherwise, each of the four types of membrane elements was used for individual CD configuration.

3.2. SWRO model simulation results

Fig. 3 illustrates the SWRO model simulation results for each element configuration in the pressure vessel. Monitoring data, described in Section 2.1, were used as input data to simulate the SWRO model depending on the fluctuations in seawater temperature and TDS concentration. CD 1 had the lowest SEC mean value due to the high permeate flowrate. The mean recovery ratio for CD 1 was 44%, which was the highest value among all configurations. In the case of other CD configurations, energy consumption gradually increased when changing a high flux configuration (such as that with HF 1) to a high rejection configuration (such as that with HR 1). The decrease in water permeability led to a decrease in SEC in the constant operating pressure mode. Although the mean recovery ratio values for CD 3 and CD 4 were less than 40%, they were more advantageous with respect to permeate water quality. However, all of the selected ISD configurations displayed very stable performance with adequate levels of energy consumption, water recovery, and permeate TDS concentration regardless of their element combinations. They had an SEC mean value of 2.1 kWh/m^3. Although they had a higher SEC than those of CD 1 and CD 2, their standard deviation was smaller than that of CD 1. They maintained a mean recovery ratio value of around 40% and showed a similar TDS concentration to those of CD 3 and CD 4.

3.3. Cleaning frequency for each element configuration

Fig. 4 describes the cleaning frequency for eight configurations over the simulation period of 12 months. Although the parameters for the cleaning criteria in the SWRO simulation were set according to both SEC and permeate TDS concentration, SEC was the more important factor in deciding an appropriate time to clean reverse osmosis membranes in all configurations but CD 1. Membrane cleaning for CD 1 was first started 96 d into the simulation. CD 2 to CD 4 and ISD 1 to ISD 4 were reached on the cleaning criteria over time. As expected, configurations with only high flux membranes required more frequent membrane cleaning. CD 1 and CD 2 required cleaning more than three times a year. In contrast, cleaning for high rejection membranes and ISD all occurred twice a year. CD 4 showed the best performance among CD configurations in terms of the cleaning schedule. ISD 3 and ISD 4 had the longest operation periods between cleaning

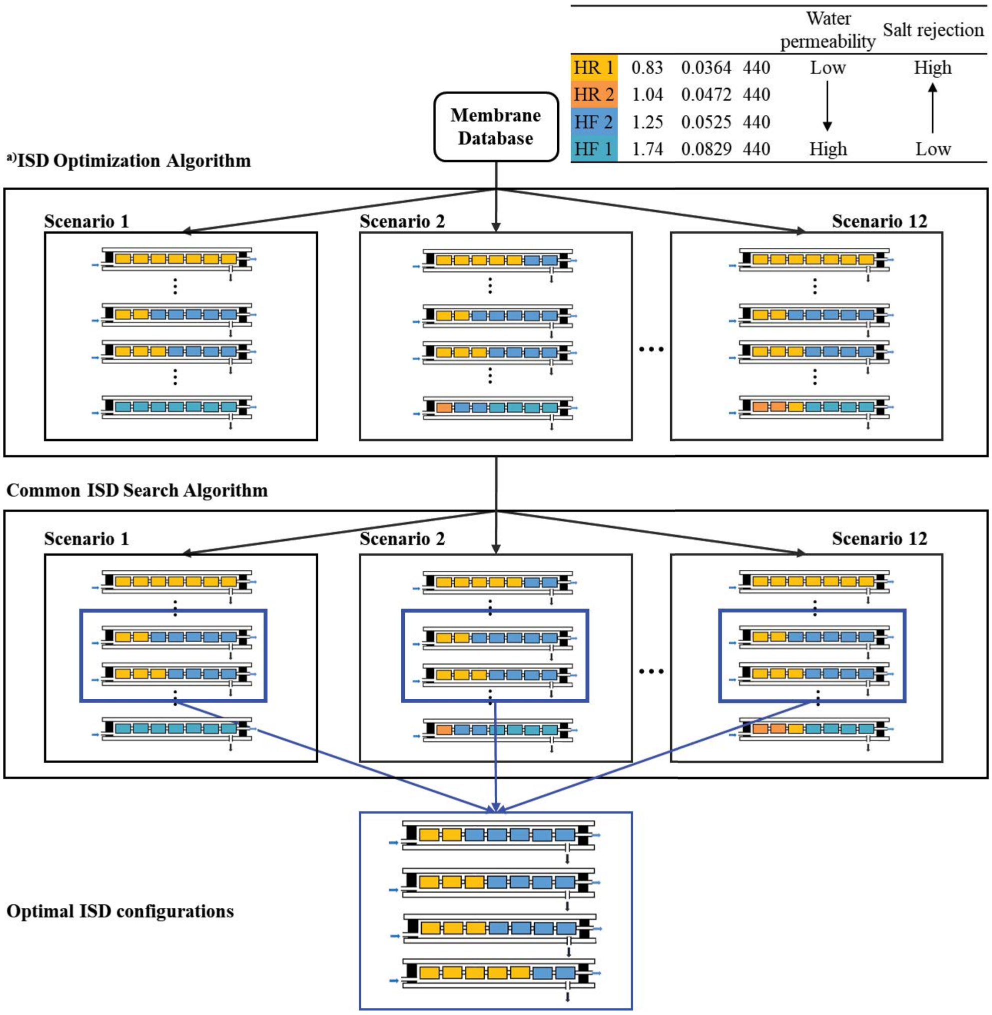

Fig. 2. Graphical summary of the internally staged design (ISD) optimization algorithm depending on the seasonal variations of seawater quality; HR: high rejection membrane; HF: high flux membrane; [a]ISD optimization algorithm using the pattern search algorithm developed in our previous study.

Table 2
ISD configurations for each month and common ISD configurations for all months

Month	Monthly mean of TDS concentration (mg/L)	Monthly mean of temperature (°C)	Number of ISD configurations for each month	Number of common ISD configurations for all months
February	36,500	23.85	17	
March	36,577	24.58	18	
April	36,733	27.21	16	
May	36,867	30.64	12	
June	37,037	33.03	8	
July	37,106	32.12	8	
August	37,271	31.58	9	4
September	37,161	31.75	9	
October	36,960	31.19	12	
November	36,827	28.97	15	
December	36,558	26.59	16	
January	36,588	26.94	16	

Table 3
Conventional design (CD) and ISD element configuration from the ISD optimization algorithm

Element configuration	Element type						
	1	2	3	4	5	6	7
				CD			
CD 1	HF 1	HF 1	HF 1	HF 1	HF 1	HF 1	HF 1
CD 2	HF 2	HF 2	HF 2	HF 2	HF 2	HF 2	HF 2
CD 3	HR 2	HR 2	HR 2	HR 2	HR 2	HR 2	HR 2
CD 4	HR 1	HR 1	HR 1	HR 1	HR 1	HR 1	HR 1
				ISD			
ISD 1	HR 1	HR 1	HF 2	HF 2	HF 2	HF 2	HF 2
ISD 2	HR 1	HR 1	HR 1	HF 2	HF 2	HF 2	HF 2
ISD 3	HR 1	HR 1	HR 1	HR 1	HF 2	HF 2	HF 2
ISD 4	HR 1	HR 1	HR 1	HR 1	HR 1	HF 2	HF 2

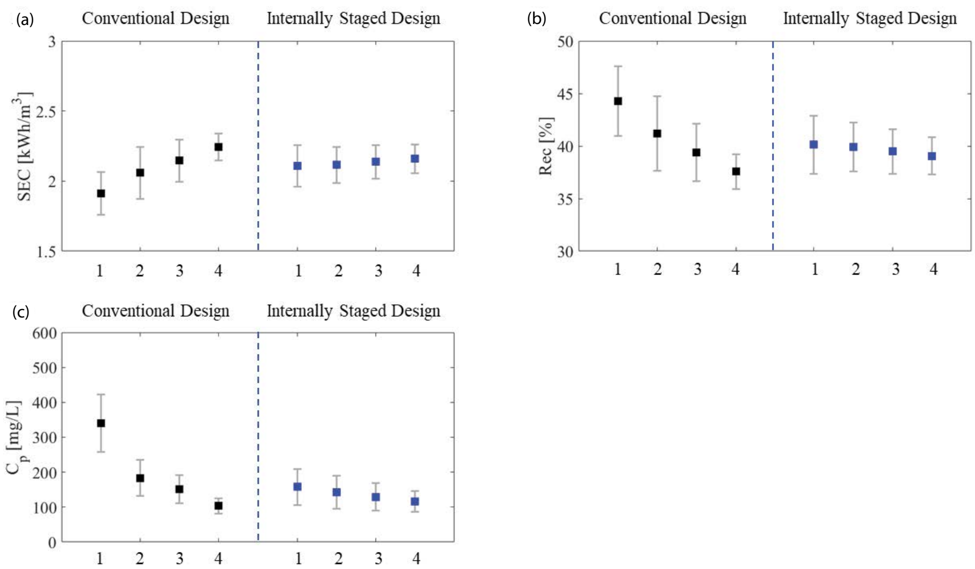

Fig. 3. Seawater reverse osmosis (SWRO) model simulation results for each element configuration: (a) specific energy consumption (kWh/m^3), (b) recovery ratio (%), and (c) permeate TDS concentration (mg/L). The squares indicate the mean of each parameter. The error bars represent one standard deviation above and below the mean values.

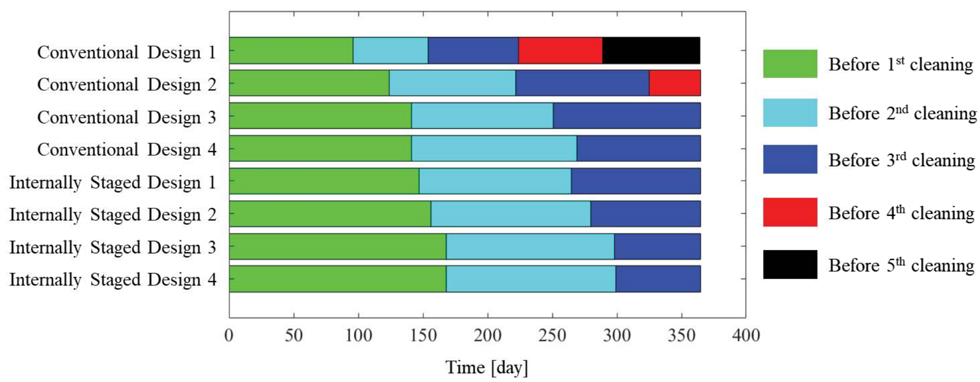

Fig. 4. Cleaning schedules depending on the membrane configuration. Different colors indicate the operation periods of the SWRO process before membrane cleanings.

operations by a wide margin. The difference between the second cleaning operations of CD 4 and ISD 3 was only 30 d.

4. Conclusions

This study was designed to evaluate the stability of ISD configurations under variations of feed water temperature and TDS concentration using seawater monitoring data. The optimization algorithm developed in a previous study was employed to derive element configurations in a pressure vessel. The monthly means of seawater temperature and TDS concentration were employed to identify optimum ISD configurations. The monitoring data were treated using a linear interpolation method to test the changes in the performance of SWRO on a daily basis. From this study, the following conclusions can be drawn:

- Four ISD configurations were generated by the optimization algorithm. The combination of two types of membrane was enough to meet the design criteria under seasonal variations of seawater quality and temperature.
- High flux and high rejection membrane configurations had advantages with respect to recovery ratio and permeate water quality, respectively. However, ISD configurations had similar performance with both high flux and high rejection membranes. It is advantageous that the SEC of ISD configurations had similar performance to that of high flux membrane configurations, and they resembled the performance of high rejection membrane configurations in terms of permeate water quality.
- ISD configurations showed remarkable performance in terms of cleaning schedule compared to CD configurations. ISD configurations were more stable to the seasonal variations of seawater temperature and TDS concentration and met the performance requirements for the monthly mean values thereof.

Acknowledgments

This work was supported by the Korea Environment Industry & Technology Institute (KEITI) through the Industrial Facilities & Infrastructure Research Program and funded by the Republic of Korea Ministry of Environment (MOE) (1485016428). We would also like to thank Doosan Heavy Industries & Construction for providing experimental data from the Fujairah plant in the United Arab Emirates.

Symbols

A — Water transport coefficient, L/m² h bar
a_T — Temperature coefficient for TCF_A, K
B — Salt transport coefficient, L/m² h
b_T — Temperature coefficient for TCF_B, K
c — Concentration, mg/L
d_p — Diameter of colloidal foulant, m
H — Channel height, m
k — Mass transfer coefficient
k^* — Cake-hindered mass transfer coefficient
k_{fp} — Colloidal fouling potential coefficient
$k_{friction}$ — Friction coefficient
L — Channel length, m
M — Molecular weight, g/mol
m_d — Deposited foulant mass per unit area, kg/m²
N — Total number of membrane elements
N_{ion} — Ionization number of the solution
p — Pressure, bar
Q — Volumetric flow rate, m³/d
R — Hydraulic resistance, m⁻¹
R_g — Ideal gas constant, cm³ bar/mol K
T — Temperature, K
TCF — Temperature correction factor
T_{ref} — Reference temperature, K
v_w — Water flux, m³/m² s
v_s — Salt flux, kg/m² s
w — Membrane channel width, m
W_{HP} — Work done by the high-pressure pump, kW
W_{BP}^{ERD} — Work done by booster pump, kW
x — Distance along the membrane channel

Greek symbols

μ — Viscosity, Pa s
ε — Porosity
ρ — Particle density of colloidal foulant
π — Osmotic pressure, bar
ξ — Dummy variable for the integration of distance x
τ — Dummy variable for the integration of time t
η_{HP} — Efficiency of high-pressure pump, %
η_{BP} — Efficiency of the booster pump, %
η_{ERD} — Efficiency of ERD, %

Subscripts

A — Water permeability
B — Salt permeability
c — Cake layer
f — Feed
m — Membrane wall
p — Permeate
s — Salt
w — Water

References

[1] L.F. Greenlee, D.F. Lawler, B.D. Freeman, B. Marrot, P. Moulin, Reverse osmosis desalination: water sources, technology, and today's challenges, Water Res., 43 (2009) 2317–2348.
[2] M. Qasim, M. Badrelzaman, N.N. Darwish, N.A. Darwish, N. Hilal, Reverse osmosis desalination: a state-of-the-art review, Desalination, 459 (2019) 59–104.
[3] J.R. Werber, A. Deshmukh, M. Elimelech, The critical need for increased selectivity, not increased water permeability, for desalination membranes, Environ. Sci. Technol. Lett., 3 (2016) 112–120.
[4] J.R. Werber, C.O. Osuji, M. Elimelech, Materials for next-generation desalination and water purification membranes, Nat. Rev. Mater., 1 (2016) 16018.
[5] G.M. Geise, H.B. Park, A.C. Sagle, B.D. Freeman, J.E. McGrath, Water permeability and water/salt selectivity tradeoff in polymers for desalination, J. Membr. Sci., 369 (2011) 130–138.
[6] Y. Du, L. Xie, Y. Liu, S. Zhang, Y. Xu, Optimization of reverse osmosis networks with split partial second pass design, Desalination, 365 (2015) 365–380.
[7] Y.-Y. Lu, Y.-D. Hu, X.-L. Zhang, L.-Y. Wu, Q.-Z. Liu, Optimum design of reverse osmosis system under different feed

concentration and product specification, J. Membr. Sci., 287 (2007) 219–229.
[8] M.G. Marcovecchio, P.A. Aguirre, N.J. Scenna, Global optimal design of reverse osmosis networks for seawater desalination: modeling and algorithm, Desalination, 184 (2005) 259–271.
[9] K. Jeong, M. Park, T.H. Chong, Numerical model-based analysis of energy-efficient reverse osmosis (EERO) process: performance simulation and optimization, Desalination, 453 (2019) 10–21.
[10] Y.-Y. Lu, Y.-D. Hu, D.-M. Xu, L.-Y. Wu, Optimum design of reverse osmosis seawater desalination system considering membrane cleaning and replacing, J. Membr. Sci., 282 (2006) 7–13.
[11] A. Jiang, H. Wang, Y. Lin, W. Cheng, J. Wang, A study on optimal schedule of membrane cleaning and replacement for spiral-wound SWRO system, Desalination, 404 (2017) 259–269.
[12] K.M. Sassi, I.M. Mujtaba, Effective design of reverse osmosis based desalination process considering wide range of salinity and seawater temperature, Desalination, 306 (2012) 8–16.
[13] K.M. Sassi, I.M. Mujtaba, Optimal operation of RO system with daily variation of freshwater demand and seawater temperature, Comp. Chem. Eng., 59 (2013) 101–110.
[14] S.J. Kim, Y.G. Lee, K.H. Cho, Y.M. Kim, S. Choi, I.S. Kim, D.R. Yang, J.H. Kim, Site-specific raw seawater quality impact study on SWRO process for optimizing operation of the pressurized step, Desalination, 238 (2009) 140–157.
[15] V.G. Molina, M. Busch, P. Sehn, Cost savings by novel seawater reverse osmosis elements and design concepts, Desal. Wat. Treat., 7 (2009) 160–177.
[16] B. Peñate, L. García-Rodríguez, Reverse osmosis hybrid membrane inter-stage design: a comparative performance assessment, Desalination, 281 (2011) 354–363.
[17] K. Jeong, M. Park, S.J. Ki, J.H. Kim, A systematic optimization of internally staged design (ISD) for a full-scale reverse osmosis process, J. Membr. Sci., 540 (2017) 285–296.
[18] J. Kim, S. Hong, Optimizing seawater reverse osmosis with internally staged design to improve product water quality and energy efficiency, J. Membr. Sci., 568 (2018) 76–86.
[19] Y.G. Lee, Y.S. Lee, D.Y. Kim, M. Park, D.R. Yang, J.H. Kim, A fouling model for simulating long-term performance of SWRO desalination process, J. Membr. Sci., 401–402 (2012) 282–291.
[20] D.Y. Kim, M.H. Lee, S. Lee, J.H. Kim, D.R. Yang, Online estimation of fouling development for SWRO system using real data, Desalination, 247 (2009) 200–209.
[21] Y.G. Lee, D.Y. Kim, Y.C. Kim, Y.S. Lee, D.H. Jung, M. Park, S.-J. Park, S. Lee, D.R. Yang, J.H. Kim, A rapid performance diagnosis of seawater reverse osmosis membranes: simulation approach, Desal. Water Treat., 15 (2010) 11–19.
[22] S.J. Lim, S.J. Ki, J. Seo, S.H. Chae, Y.G. Lee, K. Jeong, J. Park, J.H. Kim, Evaluating the performance of extended and unscented Kalman filters in the reverse osmosis process, Desal. Water Treat., 163 (2019) 118–124.
[23] M. Soltanieh, W.N. Gill, Review of reverse osmosis membranes and transport models, Chem. Eng. Commun., 12 (1981) 279–363.
[24] C.J. Seeton, Viscosity–temperature correlation for liquids, Tribol. Lett., 22 (2006) 67–78.
[25] W. Zhou, L. Song, T.K. Guan, A numerical study on concentration polarization and system performance of spiral wound RO membrane modules, J. Membr. Sci., 271 (2006) 38–46.
[26] K.L. Chen, L. Song, S.L. Ong, W.J. Ng, The development of membrane fouling in full-scale RO processes, J. Membr. Sci., 232 (2004) 63–72.
[27] T.H. Chong, F.S. Wong, A.G. Fane, Implications of critical flux and cake enhanced osmotic pressure (CEOP) on colloidal fouling in reverse osmosis: Experimental observations, J. Membr. Sci., 314 (2008) 101–111.
[28] M. Park, J. Lee, C. Boo, S. Hong, S.A. Snyder, J.H. Kim, Modeling of colloidal fouling in forward osmosis membrane: effects of reverse draw solution permeation, Desalination, 314 (2013) 115–123.
[29] E.M.V. Hoek, M. Elimelech, Cake-enhanced concentration polarization: a new fouling mechanism for salt-rejecting membranes, Environ. Sci. Technol., 37 (2003) 5581–5588.
[30] G. Schock, A. Miquel, Mass transfer and pressure loss in spiral wound modules, Desalination, 64 (1987) 339–352.
[31] A. Ghobeity, A. Mitsos, Optimal time-dependent operation of seawater reverse osmosis, Desalination, 263 (2010) 76–88.